






Endowing the Ising superconductor NbSe₂ with nontrivial band topology via proximity coupling with the two-dimensional ferromagnet Fe₃GeTe₂

Yutong Yang ^{1,2}, Wei Qin ³, Yanru Chen,^{1,2} Shunhong Zhang ^{1,2}, Ping Cui ^{1,2,*} and Zhenyu Zhang ^{1,2,†}

¹*International Center for Quantum Design of Functional Materials (ICQD), Hefei National Research Center for Physical Sciences at the Microscale, University of Science and Technology of China, Hefei, Anhui 230026, China*

²*Hefei National Laboratory, University of Science and Technology of China, Hefei, Anhui 230088, China*

³*Department of Physics, University of Science and Technology of China, Hefei, Anhui 230026, China*



(Received 29 October 2023; accepted 4 January 2024; published 26 January 2024)

Using first-principles calculations combined with the Löwdin partitioning method, we investigate the layer-resolved topological properties of the Ising superconductor NbSe₂ proximity coupled with a two-dimensional metallic ferromagnet Fe₃GeTe₂ (FGT). We first reveal that the top NbSe₂ monolayer develops a nontrivial band topology under the lateral compression caused by the FGT overlayer, while the remaining NbSe₂ layers maintain their band triviality. More significantly, the top NbSe₂ monolayer exhibits distinctly different band topology when the FGT magnetization is switched off or on, characterized by a topological invariant $Z_2 = 1$ or Chern number $C = 1$, respectively. We further confirm that the Ising pairing nature in the top NbSe₂ monolayer is well preserved in the heterostructure. This study not only provides an appealing candidate system for realizing topological Ising superconductivity, but also presents a generic first-principles based approach for describing topological superconductivity beyond prevailing empirical phenomenological modeling.

DOI: [10.1103/PhysRevB.109.L041112](https://doi.org/10.1103/PhysRevB.109.L041112)

Over the years, substantial efforts have been devoted to discoveries of topological superconductors, which in turn can be further exploited as building blocks for the potential realization of Majorana-based qubits and fault-tolerant quantum computing [1–10]. In this endeavor, different design schemes have been employed to realize topological superconductivity, including notably heterostructural platforms that integrate proper superconducting and other constituent materials proximity coupled with each other [11–13]. Candidate superconducting materials normally possess strong spin-orbit coupling (SOC) [13], including Ising superconductors whose Cooper pairs possess mixed spin-singlet and triplet components due to strong SOC and inversion symmetry breaking [14–22]. Signatures of unconventional orbital Fulde-Ferrell-Larkin-Ovchinnikov states have also been predicted or observed recently in Ising superconductors [23,24]. The other constituent materials that have been exploited so far include topological insulators [11,25–28], semiconducting or magnetic wires [12,29,30], and two-dimensional (2D) magnets [31–38]. In these studies, the emergence of topological superconductivity has typically been signified by the observation of Majorana zero modes as quasiparticle excitations at defective sites (e.g., superconducting vertex centers, wire ends, island edges, etc.). Yet to date, despite the extensive research efforts surrounding the various realization routes, definitive proofs of topological superconductivity such as

an unambiguous demonstration of the non-Abelian statistics obeyed by the Majorana fermions are still lacking. Given this grand challenging status of the vitally important field, new candidate materials platforms that may harbor topological superconductivity remain strongly desirable, especially those that may facilitate more convenient braiding of the resultant Majorana excitations.

Among the different classes of candidate topological superconductors based on van der Waals (vdW) heterostructures, those integrating 2D ferromagnets and Ising superconductors have gained increasing attention [39–42]. Compelling examples include the observations of Majorana modes at the edges of a semiconducting magnetic monolayered island of CrBr₃ on top of an Ising superconductor of NbSe₂ [39], and surprisingly long-distance transmission of skin Josephson currents across a metallic magnetic bridge of Fe₃GeTe₂ (FGT) connecting two NbSe₂ terminals [42]. In particular, in the latter system, competing microscopic mechanisms for the unusual transmission have been speculated, including the emergence of a spin-triplet component of the supercurrent, which in principle would characterize the system to be topologically nontrivial. Yet on the theory side, the prevailing approach to address the topological nature of such hybrid systems of magnetic and superconducting components has so far relied on phenomenological modeling [12,39,43–45], in which the treatments of both band structures and magnetic components typically invoke empirical physical parameters. It remains highly desirable, and technically also challenging, to characterize and further identify the origin of the topological nature of such given system with the equal footing accuracy of first-principles approaches.

*Corresponding author: cuipeg@ustc.edu.cn

†Corresponding author: zhangzy@ustc.edu.cn

In this Letter, we use first-principles calculations combined with the Löwdin partitioning method [46,47] to investigate the layer-resolved topological properties of a representative system consisting of an Ising superconductor of NbSe₂ proximity coupled with a ferromagnet of FGT. Given the metallic nature of both components and the resultant overpopulated bands around the Fermi level, no existing first-principles based approach can be employed to characterize the topological nature of the system. Nevertheless, the Löwdin partitioning method allows one to construct an effective model for each NbSe₂ layer by taking into account the influence of neighboring layers with first-principles accuracy (including both FGT and NbSe₂). Our studies first reveal that the top NbSe₂ monolayer closest to the FGT layer develops a non-trivial band topology due to the concerted effect of SOC and trimerized lattice distortion induced by the FGT overlayer, while the remaining NbSe₂ layers stay trivial. More significantly, by switching on or off the FGT magnetization, the band topology of the top NbSe₂ monolayer is characterized by a Chern number $C=1$ or topological invariant $Z_2=1$, respectively. These findings help to shed light on the microscopic understanding of the existing experimental observations of skin transmission effects in this system [42], and provide an appealing candidate platform for realizing topological Ising superconductivity. Furthermore, the approach demonstrated here for characterizing topological superconductivity beyond the prevailing empirical phenomenological modeling method [12,39,43–45] should find broad applicability in other related systems.

We first obtain the structural, magnetic, and electronic properties within density functional theory (DFT), and the WANNI90 package [48,49] is then utilized to construct the real-space Hamiltonian $H(\vec{R})$. In stark contrast to a typical topological insulator characterized by a well-defined global band gap over the Brillouin zone (BZ), the intricate band structure around the Fermi level of FGT/NbSe₂ (see Fig. 1) hinders straightforward calculations of the Wannier charge centers (WCCs) and associated topological invariants. To reveal the hidden topological properties, we employ the Löwdin partitioning method to construct the layer-resolved effective Hamiltonian for each NbSe₂ layer by perturbatively incorporating the influence of neighboring layers.

Since Löwdin partitioning is more convenient for carrying out in the k space in the present study, we transform $H(\vec{R})$ into $H(\vec{k})$ via Fourier transformation $H(\vec{k}) = \sum_{\vec{R}} e^{i\vec{k}\cdot\vec{R}} H(\vec{R})/N_k$, where N_k is the total number of k points [50]. The total k -space Hamiltonian $H(\vec{k})$ can be decomposed into

$$H(\vec{k}) = H^0(\vec{k}) + H'(\vec{k}), \quad (1)$$

where H^0 and H' denote the layer-diagonal and off-diagonal blocks of H , respectively. Since the interlayer interaction between either two neighboring NbSe₂ layers or NbSe₂ and FGT layers is vdW type, which is much weaker than the intralayer kinetic energy of electrons, H' can be perturbatively integrated in constructing the layer-resolved effective Hamiltonian. By implementing the Löwdin partitioning (refer to the Supplemental Material (SM) [51], which contains further method and calculation details together with the relevant references involved [52–81]), the layer-resolved effective Hamiltonian is

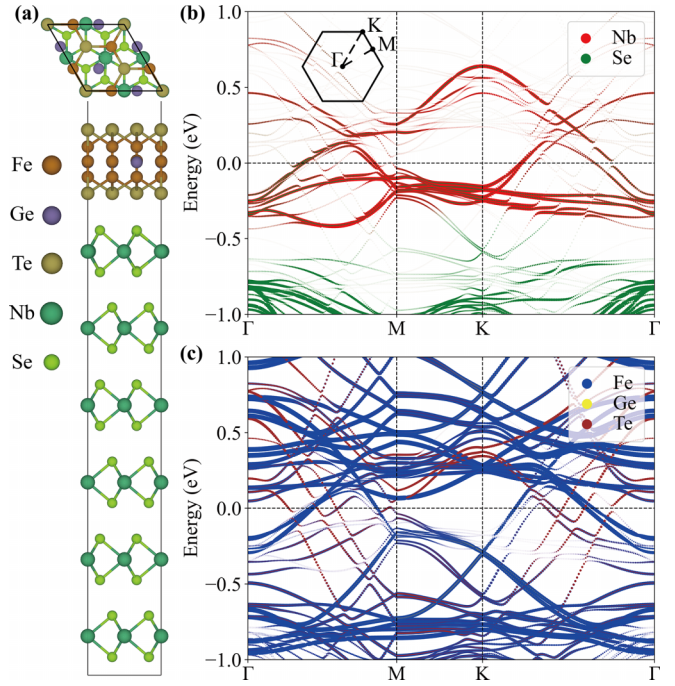


FIG. 1. (a) Top (upper panel) and side (lower panel) views of the FGT/NbSe₂ heterostructure. DFT band structures of FGT/NbSe₂ projected onto the (b) top NbSe₂ monolayer and (c) FGT overlayer, with the sizes of the colored dots representing the atom weights.

given as

$$\tilde{H}_{lm,lm'} = E_{lm}\delta_{m,m'} + \frac{1}{2} \sum_{l'n} \hat{H}'_{lm,l'n} \hat{H}'_{l'n,lm'} \times \left[\frac{1}{E_{lm} - E_{l'n}} + \frac{1}{E_{l'm'} - E_{l'n}} \right], \quad (2)$$

where l (l') and m (m', n) are the layer and band indices, respectively, $\hat{H}' = U^{-1}H'U$, $U = \{|lm\rangle\}$ is a unitary matrix that diagonalizes H^0 , and $|lm\rangle$ and E_{lm} are the corresponding eigenstate and eigenenergy.

The Löwdin partitioning method works well when the layer-diagonal energy separation between two neighboring layers is sufficiently larger than the layer-off-diagonal coupling strength. To simplify the numerical calculations, we further approximate the energy of the target layer l in Eq. (2) by the layer-averaged energy $\bar{E}_l = N_l^{-1} \sum_m E_{lm}$, where N_l is the dimension of the l th layer Hamiltonian. Equation (2) is then reduced to

$$\tilde{H}_{lm,lm'} \approx E_{lm}\delta_{m,m'} + \sum_{l'n} \hat{H}'_{lm,l'n} \hat{H}'_{l'n,lm'} \left(\frac{1}{\bar{E}_l - E_{l'n}} \right). \quad (3)$$

The validity of this approximation is reflected in Figs. 2(a) and 2(b), where the band structures obtained from Eq. (3) agree well with those obtained from the DFT calculations. Additional discussions about the validity of this method are given in the SM [51]. Once the k -space layer-resolved effective Hamiltonian in Eq. (3) is constructed, we transform it back into the Wannier basis as $H_{\text{eff}}(\vec{R}) = \sum_{\vec{k}} e^{-i\vec{k}\cdot\vec{R}} U \tilde{H}(\vec{k}) U^{-1} / N_k$, and employ WANNIERTOOLS and Z2PACK [77–80] to investigate the associated layer-resolved band topology.

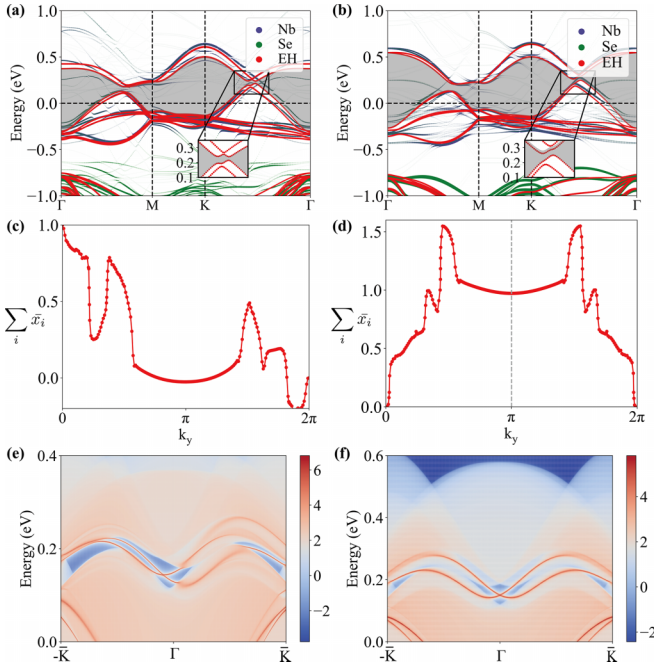


FIG. 2. (a) Projected band structures of the top NbSe₂ monolayer calculated from the DFT (blue and green dots) and effective Hamiltonian (EH, red dots) when the FGT magnetization is switched on. The sizes of the colored dots represent the atom weights. The gray area highlights the “curved” band gap. (c),(e) The corresponding summation of the hybrid WCCs as a function of k_y and topological edge states, both calculated from the EH. In (e), the warmer colors denote higher edge densities of states, while the blue regions denote the 2D bulk gaps. (b),(d),(f) Same as (a),(c),(e), but for the FGT magnetization switched off.

Before studying the electronic and topological properties, we examine the energetic, dynamic, and thermodynamic stabilities of an FGT/NbSe₂ heterostructure consisting of an FGT monolayer and three 2H-NbSe₂ bilayers. FGT is a 2D ferromagnetic metal with a high Curie temperature of 205 K in its bulk phase [33], while H-phase NbSe₂ atomic layers, especially in the monolayer limit, exhibit significant Ising superconductivity [18–22]. The lattice constants of a free-standing FGT monolayer and 2H-NbSe₂ are calculated to be 4.00 and 3.45 Å, respectively, in good agreement with earlier reported values [33,57–59]. When forming the heterostructure, a supercell consisting of $\sqrt{3} \times \sqrt{3}$ FGT and 2×2 NbSe₂ in the x - y plane is adopted, leading to a lattice mismatch of only 0.4%. To investigate the energetic stability of FGT/NbSe₂, we calculate the binding energy defined by $E_b = E_{\text{FGT}} + E_{\text{NbSe}_2} - E_{\text{hs}}$, where E_{FGT} , E_{NbSe_2} , and E_{hs} are the total energies of the FGT, NbSe₂, and FGT/NbSe₂ heterostructure, respectively. Three high-symmetric stacking configurations are considered (see Fig. S1 in the SM [51], which contains more DFT calculation details), and the most stable one is the Te-centered structure shown in Fig. 1(a), yielding the highest E_b of 1.73 eV per supercell (equivalent to 42 meV/Å²). The phonon spectrum of FGT/NbSe₂ calculated using density functional perturbation theory shows no imaginary frequency (Fig. S2 [51]), indicating that the heterostructure is dynamically stable. Moreover, our *ab initio*

molecular dynamics simulations performed at 230 K for up to 20 ps confirm the thermodynamic stability of the system (Fig. S2 [51]).

We next investigate the electronic properties of the most stable configuration of FGT/NbSe₂ based on DFT calculations and Wannier functions [50] with the inclusion of the SOC. The band structures of FGT/NbSe₂ projected onto the top NbSe₂ layer and FGT are shown in Figs. 1(b) and 1(c), respectively, both of which are metallic and pronouncedly hybridized around the Fermi level. Moreover, as shown in Fig. 1(b), band splittings are revealed at the time-reversal-invariant Γ and M points for NbSe₂, which are attributed to the magnetic proximity effect of FGT. These observations suggest that the vdW-type coupling between FGT and NbSe₂ indeed plays a crucial role in tuning both the electronic and magnetic properties of the heterostructure. However, the absence of a global or “curved” band gap over the whole BZ of FGT/NbSe₂ hampers calculations of the topological invariant from hybrid WCCs [80].

To explore the potentially hidden band topology in each layer of NbSe₂, we employ the approach introduced earlier to construct the layer-resolved effective Hamiltonian. Here, we mainly focus on the top NbSe₂ monolayer because it is proximal to the FGT overlayer. As shown in Figs. 2(a) and 2(b), the band structures calculated from the effective Hamiltonian agree well with the DFT results of the top NbSe₂ monolayer-projected band structures around the Fermi level, validating the approximation employed in constructing the layer-resolved Hamiltonian. When switching on the ferromagnetism of FGT, band splittings around the Γ and M points are also reproduced. Significantly, well-defined “curved” band gaps emerge in Figs. 2(a) and 2(b), separating the bands into “occupied” and “unoccupied” states, enabling the calculations of WCCs and the corresponding topological invariants [80].

When the FGT magnetization is on, the Chern number is calculated by $C = \bar{X}(2\pi) - \bar{X}(0)$ [78,79], where $\bar{X}(k_y) = \frac{1}{a_x} \sum_i \bar{x}_i(k_y)$, i denotes the band index, and a_x is the lattice constant along the x direction. The WCCs $\bar{x}_i(k_y)$ are assumed to be smooth functions of k_y within $k_y \in [0, 2\pi]$. When the FGT magnetization is off, the Z_2 topological invariant is given by $Z_2 = |\bar{X}(\pi) - \bar{X}(0)| \bmod 2$. Based on the effective Hamiltonian, we calculate the WCCs of the top NbSe₂ monolayer and find $C = 1$ ($Z_2 = 1$) in the on (off) case, as depicted in Figs. 2(c) and 2(d).

As another manifestation of the nontrivial band topology, we calculate the corresponding topological edge states of the top NbSe₂ monolayer, as shown in Figs. 2(e) and 2(f). When the FGT magnetization is switched on, only one topological edge state connecting the “occupied” and “unoccupied” bulk bands is present, consistent with $C = 1$. Notably, there is also a trivial edge state, which starts from the “unoccupied” bands, crosses the “curved” gap, and finally returns to the “unoccupied” bands. When the FGT magnetization is off, there are two topological edge states connecting the “occupied” and “unoccupied” bulk bands, consistent with $Z_2 = 1$. These observations are reminiscent of magnetic topological insulators [81–83], where ferromagnetism trivializes one subset of the Z_2 topological states, converting the system into quantum anomalous Hall insulators with $C = 1$.

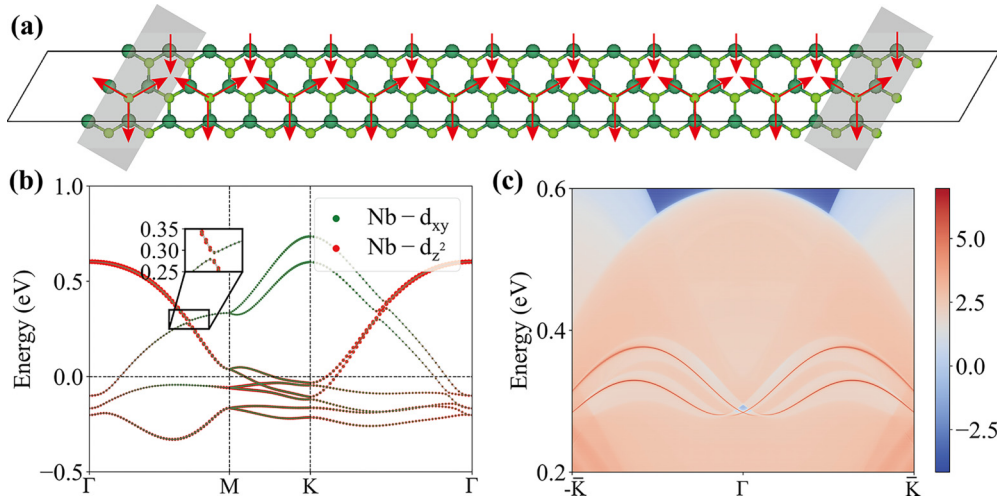


FIG. 3. (a) Lattice structure of a slab of the top NbSe₂ monolayer oriented along the [010] direction, where the red arrows indicate the trimerized lattice distortion. (b) The corresponding DFT band structure. (c) Topological edge states of the slab shown in (a), where the warmer color denotes the states at the right edge of the slab.

To reveal the origin of the nontrivial band topology of the top NbSe₂ monolayer, we isolate it from a fully relaxed FGT/NbSe₂ heterostructure to study its own electronic and topological properties via DFT calculations. As shown in Fig. 3(a), the isolated top NbSe₂ monolayer exhibits a trimerized lattice distortion due to lateral compression caused by FGT, forming a 2×2 reconstructed structure. With the inclusion of SOC, a gap is opened between the two intersecting bands characterized by the d_{z^2} and d_{xy} orbitals of Nb, as illustrated in Fig. 3(b). Notably, the band structures of a normal 2×2 NbSe₂ supercell are compared in Fig. S3 [51], showing that the band crossings due to band folding cannot be gapped by the SOC without lattice distortion. Given the existence of time-reversal symmetry and a “curved” band gap, we can calculate the Z_2 topological invariant of the system and find $Z_2 = 1$. Moreover, as shown in Fig. 3(c), Dirac-cone-like topological edge states are revealed along the [010] direction in the slab structure. Based on these results, we reach the conclusion that the emergence of the nontrivial band topology in the top NbSe₂ monolayer arises from the concerted effect of the trimerized lattice distortion and SOC.

In addition to the top NbSe₂ monolayer, we also construct the layer-resolved effective Hamiltonians of the second to sixth NbSe₂ layers, with the resulting band structures shown in Fig. S5 [51]. We find that only the top NbSe₂ monolayer opens a “curved” band gap and possesses the nontrivial band topology. Indeed, the binding energy between FGT and the top NbSe₂ layer and that between any two of the rest of the NbSe₂ layers are calculated to be 42 and 28 meV/Å², respectively, indicating a stronger interaction in the former case. Consequently, the top NbSe₂ layer exhibits the distinct trimerized lattice distortion, which further induces the nontrivial band topology, while the rest of the NbSe₂ layers stay trivial. This is because the trimerized lattice distortion occurs only in the top NbSe₂ monolayer due to the direct proximity effect of FGT.

Earlier studies demonstrated that NbSe₂ atomic layers are Ising superconductors characterized by high in-plane critical magnetic fields (H_{c2}^{\parallel}) that well exceed the corresponding

Pauli paramagnetic limits (H_p) [18–22]. For the FGT/NbSe₂ heterostructure, the FGT overlayer inevitably affects the electrical potential environment surrounding the top NbSe₂ monolayer, and thus, in principle, could alter the strength of the Ising SOC. The more recent experimental observation of superconductivity in the FGT overlayer of FGT/NbSe₂ [42] indicates that superconductivity in the top NbSe₂ monolayer must persist. Here, we explore the robustness of the Ising pairing character in the top NbSe₂ monolayer by assuming that its superconductivity is preserved. In particular, we calculate H_{c2}^{\parallel} using the pair breaking formula [84–86]

$$\ln\left(\frac{T}{T_c}\right) + \psi\left(\frac{1}{2} + \frac{\mu_B H_{c2}^{\parallel 2} / H_{\text{SOC}}}{2\pi k_B T}\right) - \psi\left(\frac{1}{2}\right) = 0, \quad (4)$$

where T_c is the superconducting critical temperature without the in-plane magnetic field, $\psi(x)$ is the digamma function, μ_B is the Bohr magneton, k_B is the Boltzmann constant, and $H_{\text{SOC}} = \Delta_{\text{SOC}} / 2\mu_B$ with Δ_{SOC} the SOC energy splitting averaged over the Fermi surface. The spin-projected Fermi surface of the top NbSe₂ monolayer is depicted in Fig. 4(a), where the associated Δ_{SOC} is estimated to be 49 meV. In Fig. 4(c), we show the temperature dependence of the in-plane critical magnetic field for different T_c , with 5.4 K being the experimentally reported value [42]. When the temperature is far below T_c ,

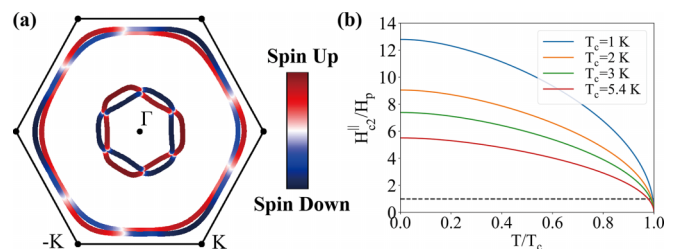


FIG. 4. (a) Spin-projected Fermi surface of the top NbSe₂ monolayer. (b) Temperature dependence of the in-plane critical field H_{c2}^{\parallel} for different T_c .

our calculations show that $H_{c2}^{\parallel}/H_p \gg 1$, indicating that the Pauli paramagnetic limit H_p [87] is strongly surpassed. Therefore, the Ising pairing nature in the top NbSe₂ monolayer is robust against the presence of the ferromagnetic FGT overlayer.

Before closing, we briefly discuss the feasibility of realizing topological Ising superconductivity in the FGT/NbSe₂ heterostructure. By taking advantage of the layer-resolved effective Hamiltonian, we demonstrate that the top NbSe₂ monolayer possesses a nontrivial band topology characterized by $C = 1$ and the topological chiral edge state. Even though this topological edge state is located at ~ 0.2 eV above the Fermi level, it can participate in the superconductivity under proper electron doping [88] or electric gating [89,90] of the samples. Earlier studies [28,81,91,92] showed that the layer-resolved chiral edge state is likely to survive in vdW-type heterostructures due to the lack of backscattering channels. Combined with the more recent experimental observation of superconductivity in the FGT/NbSe₂ heterostructure [42], this system can therefore harbor both the chiral edge state and Ising superconductivity, providing a compelling platform for realizing a topological Ising superconductor along its quasi-one-dimensional edges. Based on the present study, two aspects are crucial in designing topological superconductors consisting of vdW heterostructures. First, the interfacial vdW coupling should be strong enough to induce stable lattice distortions in the underlying superconducting layer or layers to promote the emergence of a nontrivial band topology [93]. Secondly, the superconducting substrate, e.g., NbSe₂, should contain multiple layers to ensure that the interface is superconducting, which in turn can give rise to topological edge states and Majorana excitations. These considerations

may also find relevance in other closely related vdW heterostructures consisting of 2D semiconducting magnets and 2D superconductors [94–96].

In conclusion, we have investigated the layer-resolved topological properties of the Ising superconductor NbSe₂ proximity coupled to the 2D ferromagnet FGT and found that the top NbSe₂ monolayer develops a nontrivial band topology, while the remaining NbSe₂ layers maintain their band triviality. The nontrivial band topology arises from the concerted effect of the SOC in NbSe₂ and trimerized lattice distortion caused by the FGT overlayer, characterized by $Z_2 = 1$ in the absence of ferromagnetism. By switching on the FGT magnetization, the band topology of the top NbSe₂ monolayer is converted from $Z_2 = 1$ to $C = 1$. We have also demonstrated that the Ising pairing nature is well preserved in the top NbSe₂ monolayer. These findings help to shed light on the microscopic understanding of the existing experimental observations in FGT/NbSe₂ and related systems and provide appealing platforms for realizing topological Ising superconductivity. Moreover, the generic approach demonstrated here, beyond the prevailing empirical phenomenological treatments of topological superconductivity, may find broad applicability in other related systems.

The authors thank Yuyuan Huang, Ze Huang, and Guohua Cao for helpful discussions. This work is supported by the Innovation Program for Quantum Science and Technology (Grant No. 2021ZD0302800), National Natural Science Foundation of China (Grants No. 11974323, No. 12004368, and No. 12374458), Anhui Initiative in Quantum Information Technologies (Grant No. AHY170000), and China Postdoctoral Science Foundation (Grant No. 2020M671895).

-
- [1] X.-L. Qi and S.-C. Zhang, Topological insulators and superconductors, *Rev. Mod. Phys.* **83**, 1057 (2011).
- [2] A. Yu. Kitaev, Fault-tolerant quantum computation by anyons, *Ann. Phys.* **303**, 2 (2003).
- [3] J. Alicea, New directions in the pursuit of Majorana fermions in solid state systems, *Rep. Prog. Phys.* **75**, 076501 (2012).
- [4] M. Sato and Y. Ando, Topological superconductors: A review, *Rep. Prog. Phys.* **80**, 076501 (2017).
- [5] C. W. J. Beenakker, Search for Majorana fermions in superconductors, *Annu. Rev. Condens. Matter Phys.* **4**, 113 (2013).
- [6] M. Leijnse and K. Flensberg, Introduction to topological superconductivity and Majorana fermions, *Semicond. Sci. Technol.* **27**, 124003 (2012).
- [7] T. D. Stanescu and S. Tewari, Majorana fermions in semiconductor nanowires: Fundamentals, modeling, and experiment, *J. Phys.: Condens. Matter* **25**, 233201 (2013).
- [8] S. R. Elliott and M. Franz, *Colloquium: Majorana fermions in nuclear, particle, and solid-state physics*, *Rev. Mod. Phys.* **87**, 137 (2015).
- [9] Y. Li and Z. Xu, Exploring topological superconductivity in topological materials, *Adv. Quantum Technol.* **2**, 180012 (2019).
- [10] M. M. Sharma, P. Sharma, N. K. Karn, and V. P. S. Awana, Comprehensive review on topological superconducting materials and interfaces, *Supercond. Sci. Technol.* **35**, 083003 (2022).
- [11] L. Fu and C. L. Kane, Superconducting proximity effect and Majorana fermions at the surface of a topological insulator, *Phys. Rev. Lett.* **100**, 096407 (2008).
- [12] J. D. Sau, R. M. Lutchyn, S. Tewari, and S. D. Sarma, Generic new platform for topological quantum computation using semiconductor heterostructures, *Phys. Rev. Lett.* **104**, 040502 (2010).
- [13] W. Qin, J. Gao, P. Cui, and Z. Zhang, Two-dimensional superconductors with intrinsic p -wave pairing or nontrivial band topology, *Sci. China Phys., Mech. Astron.* **66**, 267005 (2023).
- [14] J. M. Lu, O. Zheliuk, I. Leermakers, N. F. Q. Yuan, U. Zeitler, K. T. Law, and J. T. Ye, Evidence for two-dimensional Ising superconductivity in gated MoS₂, *Science* **350**, 1353 (2015).
- [15] J. Lu, O. Zheliuk, Q. Chen, I. Leermakers, N. E. Hussey, U. Zeitler, and J. Ye, Full superconducting dome of strong Ising protection in gated monolayer WS₂, *Proc. Natl. Acad. Sci. USA* **115**, 3551 (2018).
- [16] Y. Saito, Y. Nakamura, M. S. Bahramy, Y. Kohama, J. Ye, Y. Kasahara, Y. Nakagawa, M. Onga, M. Tokunaga, T. Nojima, Y. Yanase, and Y. Iwasa, Superconductivity protected by spin-valley locking in ion-gated MoS₂, *Nat. Phys.* **12**, 144 (2016).
- [17] X. Xi, Z. Wang, W. Zhao, J.-H. Park, K. T. Law, H. Berger, L. Forró, J. Shan, and K. F. Mak, Ising pairing in superconducting NbSe₂ atomic layers, *Nat. Phys.* **12**, 139 (2016).

- [18] Y. Xing, K. Zhao, P. Shan, F. Zheng, Y. Zhang, H. Fu, Y. Liu, M. Tian, C. Xi, H. Liu, J. Feng, X. Lin, S. Ji, X. Chen, Q.-K. Xue, and J. Wang, Ising superconductivity and quantum phase transition in macro-size monolayer NbSe₂, *Nano Lett.* **17**, 6802 (2017).
- [19] Y. Xing, P. Yang, J. Ge, J. Yan, J. Luo, H. Ji, Z. Yang, Y. Li, Z. Wang, Y. Liu, F. Yang, P. Qiu, C. Xi, M. Tian, Y. Liu, X. Lin, and J. Wang, Extrinsic and intrinsic anomalous metallic states in transition metal dichalcogenide Ising superconductors, *Nano Lett.* **21**, 7486 (2021).
- [20] S. C. de la Barrera, M. R. Sinko, D. P. Gopalan, N. Sivadas, K. L. Seyler, K. Watanabe, T. Taniguchi, A. W. Tsun, X. Xu, D. Xiao, and B. M. Hunt, Tuning Ising superconductivity with layer and spin-orbit coupling in two-dimensional transition-metal dichalcogenides, *Nat. Commun.* **9**, 1427 (2018).
- [21] D. Wickramaratne, S. Khmelevskiy, D. F. Agterberg, and I. I. Mazin, Ising superconductivity and magnetism in NbSe₂, *Phys. Rev. X* **10**, 041003 (2020).
- [22] L. Li, S. Zhang, G. Hu, L. Guo, T. Wei, W. Qin, B. Xiang, C. Zeng, Z. Zhang, and P. Cui, Converting a monolayered NbSe₂ into an Ising superconductor with nontrivial band topology via physical or chemical pressuring, *Nano Lett.* **22**, 6767 (2022).
- [23] Y.-M. Xie and K. T. Law, Orbital Fulde-Ferrell pairing state in moiré Ising superconductors, *Phys. Rev. Lett.* **131**, 016001 (2023).
- [24] P. Wan, O. Zheliuk, N. F. Q. Yuan, X. Peng, L. Zhang, M. Liang, U. Zeitler, S. Wiedmann, N. E. Hussey, T. T. M. Palstra, and J. Ye, Orbital Fulde-Ferrell-Larkin-Ovchinnikov state in an Ising superconductor, *Nature (London)* **619**, 46 (2023).
- [25] M.-X. Wang, C. Liu, J.-P. Xu, F. Yang, L. Miao, M.-Y. Yao, C. L. Gao, C. Shen, X. Ma, X. Chen, Z.-A. Xu, Y. Liu, S.-C. Zhang, D. Qian, J.-F. Jia, and Q.-K. Xue, The coexistence of superconductivity and topological order in the Bi₂Se₃ thin films, *Science* **336**, 52 (2012).
- [26] S. V. Eremin, V. N. Men'shov, V. V. Tugushev, P. M. Echenique, and E. V. Chulkov, Magnetic proximity effect at the three-dimensional topological insulator/magnetic insulator interface, *Phys. Rev. B* **88**, 144430 (2013).
- [27] J.-P. Xu, C. Liu, M.-X. Wang, J. Ge, Z.-L. Liu, X. Yang, Y. Chen, Y. Liu, Z.-A. Xu, C.-L. Gao, D. Qian, F.-C. Zhang, Q.-K. Xue, and J.-F. Jia, Artificial topological superconductor by the proximity effect, *Phys. Rev. Lett.* **112**, 217001 (2014).
- [28] H.-H. Sun, K.-W. Zhang, L.-H. Hu, C. Li, G.-Y. Wang, H.-Y. Ma, Z.-A. Xu, C.-L. Gao, D.-D. Guan, Y.-Y. Li, C. Liu, D. Qian, Y. Zhou, L. Fu, S.-C. Li, F.-C. Zhang, and J.-F. Jia, Majorana zero mode detected with spin selective Andreev reflection in the vortex of a topological superconductor, *Phys. Rev. Lett.* **116**, 257003 (2016).
- [29] S. Nadj-Perge, I. K. Drozdov, J. Li, H. Chen, S. Jeon, J. Seo, A. H. MacDonald, B. A. Bernevig, and A. Yazdani, Observation of Majorana fermions in ferromagnetic atomic chains on a superconductor, *Science* **346**, 602 (2014).
- [30] J. Li, H. Chen, I. K. Drozdov, A. Yazdani, B. A. Bernevig, and A. H. MacDonald, Topological superconductivity induced by ferromagnetic metal chains, *Phys. Rev. B* **90**, 235433 (2014).
- [31] B. Huang, G. Clark, E. Navarro-Moratalla, D. R. Klein, R. Cheng, K. L. Seyler, D. Zhong, E. Schmidgall, M. A. McGuire, D. H. Cobden, W. Yao, D. Xiao, P. Jarillo-Herrero, and X. Xu, Layer-dependent ferromagnetism in a van der Waals crystal down to the monolayer limit, *Nature (London)* **546**, 270 (2017).
- [32] C. Gong, L. Li, Z. Li, H. Ji, A. Stern, Y. Xia, T. Cao, W. Bao, C. Wang, Y. Wang, Z. Q. Qiu, R. J. Cava, S. G. Louie, J. Xia, and X. Zhang, Discovery of intrinsic ferromagnetism in two-dimensional van der Waals crystals, *Nature (London)* **546**, 265 (2017).
- [33] Y. Deng, Y. Yu, Y. Song, J. Zhang, N. Z. Wang, Z. Sun, Y. Yi, Y. Z. Wu, S. Wu, J. Zhu, J. Wang, X. H. Chen, and Y. Zhang, Gate-tunable room-temperature ferromagnetism in two-dimensional Fe₃GeTe₂, *Nature (London)* **563**, 94 (2018).
- [34] Z. Zhang, J. Shang, C. Jiang, A. Rasmita, W. Gao, and T. Yu, Direct photoluminescence probing of ferromagnetism in monolayer two-dimensional CrBr₃, *Nano Lett.* **19**, 3138 (2019).
- [35] D. Ghazaryan, M. T. Greenaway, Z. Wang, V. H. Guaroichico-Moreira, I. J. Vera-Marun, J. Yin, Y. Liao, S. V. Morozov, O. Kristanovski, A. I. Lichtenstein, M. I. Katsnelson, F. Withers, A. Mishchenko, L. Eaves, A. K. Geim, K. S. Novoselov, and A. Misra, Magnon-assisted tunnelling in van der Waals heterostructures based on CrBr₃, *Nat. Electron.* **1**, 344 (2018).
- [36] M. Bonilla, S. Kolekar, Y. Ma, H. C. Diaz, V. Kalappattil, R. Das, T. Eggers, H. R. Gutierrez, M.-H. Phan, and M. Batzill, Strong room-temperature ferromagnetism in VSe₂ monolayers on van der Waals substrates, *Nat. Nanotechnol.* **13**, 289 (2018).
- [37] D. J. O'Hara, T. Zhu, A. H. Trout, A. S. Ahmed, L. Yunqiu, C. H. Lee, M. R. Brenner, S. Rajan, J. A. Gupta, D. W. McComb, and R. K. Kawakami, Room temperature intrinsic ferromagnetism in epitaxial manganese selenide films in the monolayer limit, *Nano Lett.* **18**, 3125 (2018).
- [38] Y. Gong, J. Guo, J. Li, K. Zhu, M. Liao, X. Liu, Q. Zhang, L. Gu, L. Tang, X. Feng, D. Zhang, W. Li, C. Song, L. Wang, P. Yu, X. Chen, Y. Wang, H. Yao, W. Duan, Y. Xu, S.-C. Zhang, X. Ma, Q.-K. Xue, and K. He, Experimental realization of an intrinsic magnetic topological insulator, *Chin. Phys. Lett.* **36**, 076801 (2019).
- [39] S. Kezilebieke, M. N. Huda, V. Vaño, M. Aapro, S. C. Ganguli, O. J. Silveira, S. Glodzik, A. S. Foster, T. Ojanen, and P. Liljeroth, Topological superconductivity in a van der Waals heterostructure, *Nature (London)* **588**, 424 (2020).
- [40] S. Kezilebieke, O. J. Silveira, M. N. Huda, V. Vaño, M. Aapro, S. C. Ganguli, J. Lahtinen, R. Mansell, S. Dijken, A. S. Foster, and P. Liljeroth, Electronic and magnetic characterization of epitaxial CrBr₃ monolayers on a superconducting substrate, *Adv. Mater.* **33**, 2006850 (2021).
- [41] S. Kezilebieke, V. Vaño, M. N. Huda, M. Aapro, S. C. Ganguli, P. Liljeroth, and J. L. Lado, Moiré-enabled topological superconductivity, *Nano Lett.* **22**, 328 (2022).
- [42] G. Hu, C. Wang, S. Wang, Y. Zhang, Y. Feng, Z. Wang, Q. Niu, Z. Zhang, and B. Xiang, Long-range skin Josephson supercurrent across a van der Waals ferromagnet, *Nat. Commun.* **14**, 1779 (2023).
- [43] S. Nadj-Perge, I. K. Drozdov, B. A. Bernevig, and A. Yazdani, Proposal for realizing Majorana fermions in chains of magnetic atoms on a superconductor, *Phys. Rev. B* **88**, 020407(R) (2013).
- [44] J. Klinovaja, P. Stano, A. Yazdani, and D. Loss, Topological superconductivity and Majorana fermions in RKKY systems, *Phys. Rev. Lett.* **111**, 186805 (2013).
- [45] B. Braunecker and P. Simon, Interplay between classical magnetic moments and superconductivity in quantum one-dimensional conductors: Toward a self-sustained topological Majorana phase, *Phys. Rev. Lett.* **111**, 147202 (2013).

- [46] P. Löwdin, Partitioning technique, perturbation theory, and rational approximations, *Int. J. Quantum Chem.* **21**, 69 (1982).
- [47] P.-O. Löwdin, Studies in perturbation theory. IV. Solution of eigenvalue problem by projection operator formalism, *J. Math. Phys.* **3**, 969 (1962).
- [48] G. Pizzi, V. Vitale, R. Arita, S. Blügel, F. Freimuth, G. Géranton, M. Gibertini, D. Gresch, C. Johnson, T. Koretsune, J. Ibañez-Azpiroz, H. Lee, J.-M. Lihm, D. Marchand, A. Marrazzo, Y. Mokrousov, J. I. Mustafa, Y. Nohara, Y. Nomura, L. Paulatto, S. Poncé, T. Ponweiser, J. Qiao, F. Thöle, S. S. Tsirkin, M. Wierzbowska, N. Marzari, D. Vanderbilt, I. Souza, A. A. Mostofi, and J. R. Yates, Wannier90 as a community code: New features and applications, *J. Phys.: Condens. Matter.* **32**, 165902 (2020).
- [49] A. A. Mostofi, J. R. Yates, G. Pizzi, Y.-S. Lee, I. Souza, D. Vanderbilt, and N. Marzari, An updated version of wannier90: A tool for obtaining maximally-localised Wannier functions, *Comput. Phys. Commun.* **185**, 2309 (2014).
- [50] N. Marzari, A. A. Mostofi, J. R. Yates, I. Souza, and D. Vanderbilt, Maximally localized Wannier functions: Theory and applications, *Rev. Mod. Phys.* **84**, 1419 (2012).
- [51] See Supplemental Material at <http://link.aps.org/supplemental/10.1103/PhysRevB.109.L041112> for the details of calculations and supplemental figures and tables, which includes Refs. [52–81].
- [52] P. E. Blöchl, Projector augmented-wave method, *Phys. Rev. B* **50**, 17953 (1994).
- [53] G. Kresse and D. Joubert, From ultrasoft pseudopotentials to the projector augmented-wave method, *Phys. Rev. B* **59**, 1758 (1999).
- [54] G. Kresse and J. Hafner, *Ab initio* molecular dynamics for liquid metals, *Phys. Rev. B* **47**, 558 (1993).
- [55] G. Kresse and J. Furthmüller, Efficient iterative schemes for *ab initio* total-energy calculations using a plane-wave basis set, *Phys. Rev. B* **54**, 11169 (1996).
- [56] J. P. Perdew, K. Burke, and M. Ernzerhof, Generalized gradient approximation made simple, *Phys. Rev. Lett.* **77**, 3865 (1996).
- [57] H. L. Zhuang, P. R. C. Kent, and R. G. Hennig, Strong anisotropy and magnetostriction in the two-dimensional Stoner ferromagnet Fe₃GeTe₂, *Phys. Rev. B* **93**, 134407 (2016).
- [58] H. Deiseroth, K. Aleksandrov, C. Reiner, L. Kienle, and R. K. Kremer, Fe₃GeTe₂ and Ni₃GeTe₂-Two new layered transition-metal compounds: Crystal structures, HRTEM investigations, and magnetic and electrical properties, *Eur. J. Inorg. Chem.* **2006**, 1561 (2006).
- [59] B. Chen, J. Yang, H. Wang, M. Imai, H. Ohta, C. Michioka, K. Yoshimura, and M. Fang, Magnetic properties of layered itinerant electron ferromagnet Fe₃GeTe₂, *J. Phys. Soc. Jpn.* **82**, 124711 (2013).
- [60] Y. Zhao, J. Gu, and Z. Chen, Oxygen evolution reaction on 2D ferromagnetic Fe₃GeTe₂: Boosting the reactivity by the self-reduction of surface hydroxyl, *Adv. Funct. Mater.* **29**, 1904782 (2019).
- [61] M. M. Ugeda, A. J. Bradley, Y. Zhang, S. Onishi, Y. Chen, W. Ruan, C. Ojeda-Aristizabal, H. Ryu, M. T. Edmonds, H.-Z. Tsai, A. Riss, S.-K. Mo, D. Lee, A. Zettl, Z. Hussain, Z.-X. Shen, and M. F. Crommie, Characterization of collective ground states in single-layer NbSe₂, *Nat. Phys.* **12**, 92 (2016).
- [62] Y. Saito, T. Nojima, and Y. Iwasa, Highly crystalline 2D superconductors, *Nat. Rev. Mater.* **2**, 16094 (2016).
- [63] K. Zhao, H. Lin, X. Xiao, W. Huang, W. Yao, M. Yan, Y. Xing, Q. Zhang, Z.-X. Li, S. Hoshino, J. Wang, S. Zhou, L. Gu, M. S. Bahramy, H. Yao, N. Nagaosa, Q.-K. Xue, K. T. Law, X. Chen, and S.-H. Ji, Disorder-induced multifractal superconductivity in monolayer niobium dichalcogenides, *Nat. Phys.* **15**, 904 (2019).
- [64] S. Grimme, S. Ehrlich, and L. Goerigk, Effect of the damping function in dispersion corrected density functional theory, *J. Comput. Chem.* **32**, 1456 (2011).
- [65] S. Grimme, Semiempirical GGA-type density functional constructed with a long-range dispersion correction, *J. Comput. Chem.* **27**, 1787 (2006).
- [66] M. Dion, H. Rydberg, E. Schröder, D. C. Langreth, and B. I. Lundqvist, Van der Waals density functional for general geometries, *Phys. Rev. Lett.* **92**, 246401 (2004).
- [67] J. Klimeš, D. R. Bowler, and A. Michaelides, Chemical accuracy for the van der Waals density functional, *J. Phys.: Condens. Matter.* **22**, 022201 (2010).
- [68] J. Klimeš, D. R. Bowler, and A. Michaelides, Van der Waals density functionals applied to solids, *Phys. Rev. B* **83**, 195131 (2011).
- [69] S. Grimme, J. Antony, S. Ehrlich, and H. Krieg, A consistent and accurate *ab initio* parametrization of density functional dispersion correction (DFT-D) for the 94 elements H-Pu, *J. Chem. Phys.* **132**, 154104 (2010).
- [70] H. J. Monkhorst and J. D. Pack, Special points for Brillouin-zone integrations, *Phys. Rev. B* **13**, 5188 (1976).
- [71] H. Weng, X. Dai, and Z. Fang, Transition-metal pentatelluride ZrTe₅ and HfTe₅: A paradigm for large-gap quantum spin Hall insulators, *Phys. Rev. X* **4**, 011002 (2014).
- [72] C. Fang, Y. Chen, H.-Y. Kee, and L. Fu, Topological nodal line semimetals with and without spin-orbital coupling, *Phys. Rev. B* **92**, 081201(R) (2015).
- [73] C.-S. Lian, C. Si, and W. Duan, Unveiling charge-density wave, superconductivity, and their competitive nature in two-dimensional NbSe₂, *Nano Lett.* **18**, 2924 (2018).
- [74] X. Xi, L. Zhao, Z. Wang, H. Berger, L. Forró, J. Shan, and K. F. Mak, Strongly enhanced charge-density-wave order in monolayer NbSe₂, *Nat. Nanotechnol.* **10**, 765 (2015).
- [75] G. Gye, E. Oh, and H. W. Yeom, Topological landscape of competing charge density waves in 2H-NbSe₂, *Phys. Rev. Lett.* **122**, 016403 (2019).
- [76] W.-C. Chiu, S. Mardanya, R. Markiewicz, J. Nieminen, B. Singh, T. Hakioglu, A. Agarwal, T.-R. Chang, H. Lin, and A. Bansil, Topological charge density wave in monolayer NbSe₂, [arXiv:2104.14634](https://arxiv.org/abs/2104.14634).
- [77] Q. Wu, S. Zhang, H.-F. Song, M. Troyer, and A. A. Soluyanov, WannierTools: An open-source software package for novel topological materials, *Comput. Phys. Commun.* **224**, 405 (2018).
- [78] A. A. Soluyanov and D. Vanderbilt, Computing topological invariants without inversion symmetry, *Phys. Rev. B* **83**, 235401 (2011).
- [79] D. Gresch, G. Autès, O. V. Yazyev, M. Troyer, D. Vanderbilt, B. A. Bernevig, and A. A. Soluyanov, Z2Pack: Numerical implementation of hybrid Wannier centers for identifying topological materials, *Phys. Rev. B* **95**, 075146 (2017).
- [80] Z. Wang, P. Zhang, G. Xu, L. K. Zeng, H. Miao, X. Xu, T. Qian, H. Weng, P. Richard, A. V. Fedorov, H. Ding, X. Dai, and Z. Fang, Topological nature of the FeSe_{0.5}Te_{0.5} superconductor, *Phys. Rev. B* **92**, 115119 (2015).

- [81] Y. Hou, J. Kim, and R. Wu, Magnetizing topological surface states of Bi_2Se_3 with a CrI_3 monolayer, *Sci. Adv.* **5**, eaaw1874 (2019).
- [82] C.-X. Liu, X.-L. Qi, X. Dai, Z. Fang, and S.-C. Zhang, Quantum anomalous Hall effect in $\text{Hg}_{1-y}\text{Mn}_y\text{Te}$ quantum wells, *Phys. Rev. Lett.* **101**, 146802 (2008).
- [83] C.-Z. Chang, J. Zhang, X. Feng, J. Shen, Z. Zhang, M. Guo, K. Li, Y. Ou, P. Wei, L.-L. Wang, Z.-Q. Ji, Y. Feng, S. Ji, X. Chen, J. Jia, X. Dai, Z. Fang, S.-C. Zhang, K. He, Y. Wang, L. Lu, X.-C. Ma, and Q.-K. Xue, Experimental observation of the quantum anomalous Hall effect in a magnetic topological insulator, *Science* **340**, 167 (2013).
- [84] R. A. Klemm, A. Luther, and M. R. Beasley, Theory of the upper critical field in layered superconductors, *Phys. Rev. B* **12**, 877 (1975).
- [85] J. Falson, Y. Xu, M. Liao, Y. Zang, K. Zhu, C. Wang, Z. Zhang, H. Liu, W. Duan, K. He, H. Liu, J. H. Smet, D. Zhang, and Q.-K. Xue, Type-II Ising pairing in few-layer stanene, *Science* **367**, 1454 (2020).
- [86] Y. Liu, Z. Wang, X. Zhang, C. Liu, Y. Liu, Z. Zhou, J. Wang, Q. Wang, Y. Liu, C. Xi, M. Tian, H. Liu, J. Feng, X. C. Xie, and J. Wang, Interface-induced Zeeman-protected superconductivity in ultrathin crystalline lead films, *Phys. Rev. X* **8**, 021002 (2018).
- [87] A. M. Clogston, Upper limit for the critical field in hard superconductors, *Phys. Rev. Lett.* **9**, 266 (1962).
- [88] P. Rosenzweig, H. Karakachian, D. Marchenko, K. Küster, and U. Starke, Overdoping graphene beyond the van Hove singularity, *Phys. Rev. Lett.* **125**, 176403 (2020).
- [89] V. Fatemi, S. Wu, Y. Cao, L. Bretheau, Q. D. Gibson, K. Watanabe, T. Taniguchi, R. J. Cava, and P. Jarillo-Herrero, Electrically tunable low-density superconductivity in a monolayer topological insulator, *Science* **362**, 926 (2018).
- [90] E. Sajadi, T. Palomaki, Z. Fei, W. Zhao, P. Bement, C. Olsen, S. Luescher, X. Xu, J. A. Folk, and D. H. Cobden, Gate-induced superconductivity in a monolayer topological insulator, *Science* **362**, 922 (2018).
- [91] C. Zhao, L. Li, L. Zhang, J. Qin, H. Chen, B. Xia, B. Yang, H. Zheng, S. Wang, C. Liu, Y. Li, D. Guan, P. Cui, Z. Zhang, and J. Jia, Coexistence of robust edge states and superconductivity in few-layer stanene, *Phys. Rev. Lett.* **128**, 206802 (2022).
- [92] J.-P. Xu, M.-X. Wang, Z. L. Liu, J.-F. Ge, X. Yang, C. Liu, Z. A. Xu, D. Guan, C. L. Gao, D. Qian, Y. Liu, Q.-H. Wang, F.-C. Zhang, Q.-K. Xue, and J.-F. Jia, Experimental detection of a Majorana mode in the core of a magnetic vortex inside a topological insulator-superconductor $\text{Bi}_2\text{Te}_3/\text{NbSe}_2$ heterostructure, *Phys. Rev. Lett.* **114**, 017001 (2015).
- [93] S.-H. Lee and D. Cho, Charge density wave surface reconstruction in a van der Waals layered material, *Nat. Commun.* **14**, 5735 (2023).
- [94] H. Idzuchi, F. Pientka, K.-F. Huang, K. Harada, Ö. Gül, Y. J. Shin, L. T. Nguyen, N. H. Jo, D. Shindo, R. J. Cava, P. C. Canfield, and P. Kim, Unconventional supercurrent phase in Ising superconductor Josephson junction with atomically thin magnetic insulator, *Nat. Commun.* **12**, 5332 (2021).
- [95] L. Ai, E. Zhang, J. Yang, X. Xie, Y. Yang, Z. Jia, Y. Zhang, S. Liu, Z. Li, P. Leng, X. Cao, X. Sun, T. Zhang, X. Kou, Z. Han, F. Xiu, and S. Dong, Van der Waals ferromagnetic Josephson junctions, *Nat. Commun.* **12**, 6580 (2021).
- [96] K. Kang, H. Berger, K. Watanabe, T. Taniguchi, L. Forró, J. Shan, and K. F. Mak, van der Waals π Josephson junctions, *Nano Lett.* **22**, 5510 (2022).